Oxidation of Alumina-Supported Co and Co−Pd Model Catalysts for the Fischer−Tropsch Reaction

T. Nowitzki,[†] A. F. Carlsson,[‡] O. Martyanov,[‡] M. Naschitzki,[‡] V. Zielasek,[†] T. Risse,*[,‡] M. Schmal,[§] H.-J. Freund,[‡] and M. Bäumer[†]

Institut für Angewandte und Physikalische Chemie, Universität Bremen, Postfach 330440, 28334 Bremen, Germany, Abteilung Chemische Physik, Fritz-Haber-Institut der Max-Planck-Gesellschaft, Faradayweg 4−6, 14195 Berlin, Germany, and NUCAT-COPPE/EQ, Universidade Federal do Rio de Janeiro, Ilha do Fundao, COPPE, C. P. 68502, CEP 21941, Rio de Janeiro, Brazil

Received: October 16, 2006; In Final Form: February 26, 2007

Cobalt and bimetallic Co−Pd systems are well-known Fischer−Tropsch catalysts. Compared to Co, the bimetallic systems exhibit an increased activity toward CO hydrogenation and methane conversion, attributed to resistance against oxidation. To study the oxidation behavior, model catalysts have been generated by depositing either Co or first Co and subsequently Pd onto a thin epitaxial alumina film grown on NiAl(110). Pure Co particles and bimetallic particles with a Co core and a Pd shell have been studied before and after exposure to oxygen and after thermal treatments, using X-ray photoelectron spectroscopy (XPS), temperature-programmed CO desorption (TPD), ferromagnetic resonance (FMR), and infrared reflection absorption spectroscopy (IRAS) in ultrahigh vacuum. Large doses of O_2 (1000 langmuirs; 1 langmuir = 10^{-6} Torr·s) at 300 K lead to complete oxidation of Co particles. Upon annealing to temperatures above 530 K, XPS indicates that the cobalt oxide is mostly reduced by transfer of oxygen to the alumina support, resulting in its thickening. TPD, however, indicates the existence of persistent surface oxygen species, reducing the CO adsorption energy on the particles. Exposures to small doses of O_2 (30−50 langmuirs) were also studied by a careful comparison of XPS, TPD, and FMR data. In this case, XPS indicates Co in a metallic state, whereas TPD and FMR indicate oxidic behavior. We conclude that small amounts of non-stoichiometric subsurface oxygen or subsurface and surface oxygen are present which are not detectable in the Co 2p XPS signal but have a pronounced effect on the surface chemistry and the magnetism, i.e., on certain bulk properties. In the case of bimetallic Co/Pd particles, an incomplete Pd shell on the Co particles even promotes oxygen uptake, while only a complete Pd shell inhibits oxidation.

Introduction

To efficiently make use of natural gas associated with oil production,[1−4] coal gasification,[5] gas hydrates,[6] and gas stranded in remote locations,[7−9] it is necessary to convert the gas to liquids for transportation.[10] In certain markets it is economical to liquefy natural gas[11] for transport on specially designed vessels;[12] in this case, natural gas is also the product at the point of use. Alternatively, natural gas can be converted to naphtha, diesel, and waxes in the gas to liquids (GTL) process for use as transportation fuels or additives, which is becoming more promising with process improvements.[2] Currently, the GTL process consists of first converting natural gas to syngas (CO + H_2) by partial oxidation[2] and then converting the syngas mixture to hydrocarbon liquids through the Fischer−Tropsch process using a Co-based catalyst.[13−15]

In the Fischer−Tropsch reaction, oxidation of Co has been found to be a cause for deactivation of Co supported on Al_2O_3[16,17] and in industrial formulations.[18,19] To overcome this problem, Pd has been added to Co catalysts, resulting in a higher selectivity and conversion than on Co alone.[20,22] While it has been proposed that the added Pd activates the adsorption of H_2 which spills over and reduces CoO to metallic Co,[20−28] details of the underlying, presumably complex mechanisms have not been clarified yet. As a basis, the interaction of oxygen with supported Co and Co−Pd catalysts should be understood on the atomic scale.

So far, detailed studies of Co oxidation at well-defined conditions have mainly focused on single-crystal surfaces. Surface science techniques in ultrahigh-vacuum (UHV) have shown, for example, that CoO is readily formed at room temperature (RT) on close-packed Co(0001).[29,30] For the Co-(11$\bar{2}$0) surface, the oxidation to CoO(100) has been observed[31,32] while oxygen adsorption leading to surface reconstructions is reported for Co(10$\bar{1}$0).[33] X-ray photoelectron spectroscopy (XPS) studies have observed the predominant formation of CoO also for the interaction of O_2 with polycrystalline Co at RT[34] and with a Co film on Fe(100).[35] The available results for polycrystalline and single-crystalline Co surfaces, however, are of limited value for understanding the mechanisms relevant for catalysis because real Co catalysts come as supported nanosized particles.

In the following, we will present studies at well-defined supported Co and Pd−Co nanoparticles which reveal a rather complex scheme of oxidation and reduction. An epitaxial, ∼0.5 nm thick alumina film, prepared via oxidation of a NiAl(110) single crystal,[36] is used as support for these model systems so

* Corresponding author. E-mail: risse@fhi-berlin.mpg.de.
[†] Universität Bremen.
[‡] Fritz-Haber-Institut der Max-Planck-Gesellschaft.
[§] Universidade Federal do Rio de Janeiro.

10.1021/jp066796r CCC: $37.00
Published on Web 05/27/2007

that techniques such as scanning tunneling microscopy (STM), XPS, and low-energy electron diffraction (LEED) can be applied without surface charging effects. Cobalt deposited on these films at RT nucleates at point defects, resulting in homogeneously distributed small particles with a high number density.[37−39] Pd-shell/Co-core nanoparticles can be prepared by subsequent deposition of Pd, which is more mobile than Co due to weaker metal−substrate interaction, so that the Co particles are decorated by Pd while the nucleation of indivdual Pd islands is negligible.[40−42] As demonstrated in a previous study, our model systems have turned out to be thermally stable at least up to about 500 K.[43,44]

To obtain conclusive information about accordingly prepared monometallic Co and bimetallic Co−Pd Fischer−Tropsch model catalysts, we have combined techniques sensitive to the surface layers as infrared absorption (IRAS) and temperature-programmed desorption (TPD) spectroscopy with XPS and ferromagnetic resonance (FMR) measurements, which probe properties of the entire particles. Previously, combined FMR and TPD experiments have been performed for pure Co particles supported on a single-crystal alumina surface. They showed that, after exposure to small doses of oxygen, only the outer sphere of the Co particles is oxidized, leaving a metallic, magnetic core, while, with increasing oxygen doses, the entire Co particles are oxidized until the magnetic resonance signal vanishes.[45] Here, we will give a full account on our data of oxidation and reduction cycles for supported Co nanoparticles which reveal a stable non-stoichiometric oxide component and a complex interplay of oxygen, particle surface, particle interior, and the substrate. We will show that, under oxidative conditions, it strongly depends on the morphology of bimetallic Co−Pd particles whether Pd inhibits or enhances Co oxidation.

Experimental Section

The experiments were performed in two separate UHV systems with a base pressure of 1×10^{-10} mbar. One system (FHI, Berlin) is equipped with a Bio-Rad spectrometer for IRAS, a Bruker EMX electron spin resonance spectrometer used for the FMR measurements, a quadrupole mass spectrometer (Hiden), and a triple metal evaporator (Focus EFM3T) which has been described in detail elsewhere.[46] Samples could be heated by direct current and cooled by liquid helium to about 44 K. Sample temperatures were measured using a W/Re (5 and 26% Re) thermocouple spot-welded to the NiAl(110) substrate. IRAS data were obtained by accumulating 1000 scans for the CO covered sample and the background with a resolution of 4 cm^{-1}. The second UHV system (U Bremen) comprises two compartments, one equipped with a commercial scanning probe microscope (STM/AFM system by Omicron), XPS (Leybold EA10 *plus* & VG dual anode X-ray tube), and a LEED instrument (Omicron spectaLEED). XPS data were collected at a spectrometer pass energy of 25 eV with the radiation from a Mg anode. The other compartment houses metal evaporators (Focus EFM3) and a Hiden quadrupole mass spectrometer for TPD. Samples could be cooled by liquid nitrogen to 100 K and were heated via radiation from a hot tungsten filament behind. The temperature ramp (1 K/s) for TPD was conducted by a digitally controlled power supply (Schlichting Physikalische Instrumente). NiAl(110) single-crystal samples could be transferred via a small, Omicron-type carrier plate between the two compartments, while a Ni/CrNi thermocouple, spot-welded to the sample and externally contacted by Ni and NiCr plug-socket adapters, allowed for temperature measurements.

The alumina film on the NiAl(110) single crystal was prepared by previously described methods[36,40] and the quality was checked by LEED. The Co and Pd evaporators were calibrated using a quartz microbalance. Metal was deposited on the alumina film at RT. In the following, the amount of deposited metal will be given nominally as the thickness of a hypothetical continuous metal film with bulk Co or Pd density, respectively: The notation 0.2 nm Co, for instance, corresponds to an ensemble of Co particles with a mean diameter of 2.7 nm and a mean height of 1.3 nm.

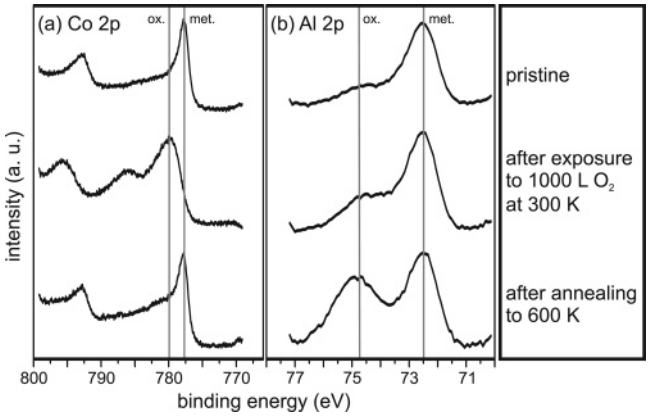

Figure 1. XP spectra for 0.4 nm Co on the alumina film (Al_2O_3/NiAl(110)). (a) Co 2p spectra: An energy of ∼778 eV as $2p_{3/2}$ peak position for the pristine sample indicates metallic Co. After oxygen exposure (large dose, 1000 langmuirs (L)) the peak has shifted to higher binding energies (∼780 eV), showing oxidation of the particles. Annealing restores the metallic spectrum, suggesting reduction of the oxide. (b) Al 2p: The spectrum for the pristine sample shows a peak at ∼72.5 eV representing metallic Al in the NiAl substrate and a shoulder at ∼75 eV belonging to oxidic Al in the alumina film. After oxygen exposure the shoulder is slightly more pronounced, indicating a thickening of the film. After subsequent annealing, the oxidic component has increased further in intensity, indicating significant thickening of the alumina film probably due to oxygen transfer from the oxidized Co particles to the NiAl support.

Results and Discussion

The XP spectrum obtained from pristine Co particles, prepared by deposition of 0.4 nm Co onto the alumina film, is shown in the top spectrum of Figure 1a. Characteristically for metallic cobalt, the Co $2p_{3/2}$ state is detected at ∼778 eV and the $2p_{1/2}$ state at ∼793 eV, respectively (see, for instance, ref 34). A CO−TPD spectrum for the as-prepared particles after saturation with 10 langmuirs (1 langmuir = 10^{-6} Torr*s) CO at 115 K is presented in Figure 2, spectrum 1. CO adsorption on the alumina substrate is observed only below 100 K so that the two desorption states, clearly observable at ∼390 and ∼270 K, represent CO species on the Co particles. As shown previously, the high-temperature peak belongs to terminally bonded CO, whereas Co carbonyls of the form $Co(CO)_n$ (n = 3, 4) are responsible for the peak at lower temperature.[47] The occurrence of carbonyls, presumably forming at low-coordinated Co sites, emphasizes that the gas interaction with Co particles is different from that with single-crystal Co surfaces such as Co(0001), where only desorption of bridge-bonded CO is detected at comparable temperatures.[48] Bridge-bonded CO, on the other hand, can be ruled out for the Co particles, because IR spectra show no intensity for such a species (see below and ref 47).

After exposing pristine Co particles to 1000 langmuirs of O_2 (large dose) at RT, both, XPS and TPD indicate that the particles are oxidized. In XPS the Co 2p peaks shift to higher binding energies (the $2p_{3/2}$ state is observed at ∼780 eV and the $2p_{1/2}$ at ∼795 eV), as the middle panel of Figure 1a shows, and a

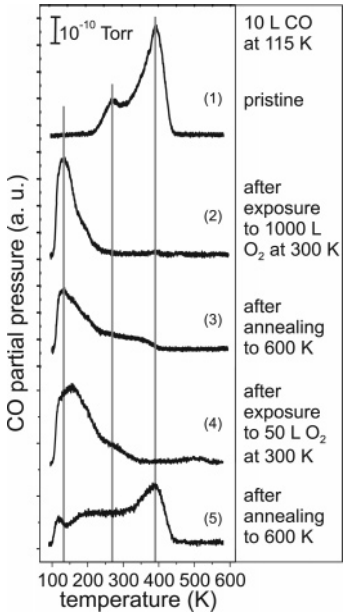

Figure 2. TPD spectra obtained after exposure of Co particles (0.4 nm Co on alumina) to 10 langmuirs of CO at 115 K. (1) Pristine particles show two desorption states: terminally bonded CO at ~390 K and a carbonyl species (Co(CO)n) at ~270 K. (2) After exposure to a large dose of oxygen (1000 langmuirs), CO desorption is completely shifted to lower temperatures, indicating smaller adsorption energies typical for CO adsorption on oxide surfaces. (3) After annealing, some intensity is regained above 300 K (typical for CO on Co) but the spectrum is dominated by desorption from cobalt oxide, contrasting the corresponding XPS results which indicate metallic Co (see Figure 1). (4) Exposure of pristine particles to only 50 langmuirs of oxygen also leads to a shift of CO desorption to lower temperatures, typical of an oxide surface. (5) Annealing of 4 results in pronounced TPD intensity at around 400 K, indicating that large portions of the surface are metallic, in contrast to 3. Still, oxidic components are clearly visible.

satellite due to shakeup becomes visible at ~785 eV, typical for cobalt oxide.[31,34] The TPD spectrum in Figure 2, spectrum 2, obtained after saturating the particles at 115 K with CO, shows no trace of desorption from metallic particles shown in Figure 2, spectrum 1. CO desorption is shifted to lower temperatures, resulting in a broad feature between 120 and 250 K. This indicates a reduction of the interaction between particles and CO, as it is expected for oxidized particles.[49,50]

The XPS and TPD spectra obtained after the oxidized particles were heated to 600 K, are shown in the bottom spectrum of Figure 1a and in Figure 2, spectrum 3, respectively. XPS suggests reduction of the cobalt oxide because the peak positions of ~778 and ~793 eV for the Co 2p levels are restored and the shakeup satellite at 785 eV has disappeared. A comparison with the spectrum obtained from the pristine sample reveals a slightly increased intensity between both metallic peaks, which may indicate a small amount of remaining cobalt oxide. The TDP spectrum, however, taken, again, after saturating the particles at 115 K with CO, shows significant desorption below 250 K characteristic for cobalt oxide, but only low intensity above 300 K, indicating that metallic Co is a minority species at the surface. On the basis of XPS and TPD alone, one might be tempted to assume that the particle core is completely reduced to metallic Co while a CoO layer remains at the surface. It will be shown later that this is not the case.

First, the processes during oxygen exposure and subsequent annealing shall be further elucidated by analyzing the XP spectra in the range of the Al 2p state (Figure 1b) indicative of the alumina support. The spectrum in the top panel, representing the sample after metal deposition, shows a peak at ~72.5 eV belonging to metallic Al in the NiAl substrate, and a shoulder at ~75 eV, characteristic for aluminum oxide in the supporting film. As visible in the middle panel, the shoulder becomes slightly more pronounced after exposing the sample to 1000 langmuirs of O_2 at 300 K (oxidation of the Co particles), indicating that the oxide film has grown thicker. A thickening of epitaxial alumina films facilitated by metal deposits has already been reported with Pd[51] or Ni[52] on top. Obviously, oxygen is dissociated on the Co particles and atomic oxygen is transferred to the support. One may speculate that only after the oxide support has reached a certain thickness, the alumina film acts as a diffusion barrier for oxygen, and the Co particles are being oxidized. Annealing the oxidized particles to 590 K even leads to further thickening of the alumina film, as revealed by a strong increase of the Al 2p XP signal from the oxide species (bottom spectrum of Figure 1b). Since the oxidation of the NiAl substrate coincides with the reduction of the particles indicated by the Co 2p spectrum (bottom spectrum of Figure 1a), there must be an efficient transfer of oxygen from the supported cobalt oxide particles to the NiAl/alumina interface upon annealing.

To study the progression of oxidation of Co particles with respect to surface and subsurface portions, small doses of O_2 in the range of 30−50 langmuirs were applied to pristine particles at RT. Figure 2, spectrum 4 shows a CO−TPD spectrum obtained after a single dose of 50 langmuirs of O_2. As for the large oxygen dose (Figure 2, spectrum 2), CO desorption is shifted to lower temperatures with a maximum at ~160 K. The TPD peak, however, appears much broader, and some intensity is observed above 250 K. Again, these particles were heated to 590 K and a CO−TPD measurement was performed. Figure 2, spectrum 5 is now dominated by desorption of terminally bonded CO on metallic Co atoms at around 390 K, but it also shows significant contributions below 200 K, characteristic for adsorption on cobalt oxide. Comparing the TPD results obtained after an oxygen exposure−annealing cycle for a large and a small dose of oxygen, we find that heating seems to remove oxygen from the particles more efficiently after exposure to a small O_2 dose, while, in both cases, the particles are not completely reduced to metallic Co.

Figure 3a shows XPS data of the Co 2p emission that were obtained from 0.2 nm Co deposited on a freshly prepared alumina film during a series of cycles of exposure to 30 langmuirs of O_2 followed by annealing to 530 K. The spectrum shown in gray was measured directly after dosing 30 langmuirs of O_2 to the sample at RT. It compares well to that of the pristine particles, indicating that the majority of Co is still metallic, contrasting the TPD data of Figure 2, spectrum 4. After completing the first cycle by annealing to 530 K, the XPS indicates a completely metallic Co deposit, and even after three cycles of oxygen exposure and annealing, the XP spectrum is essentially unaltered. After the completion of six cycles, however, a discernible cobalt oxide component is detected in the XP spectra (intensity in the shakeup region at ~785 eV), and ten cycles are obviously sufficient to completely oxidize the particles because the XP spectrum does not change upon further cycles of oxygen exposure and annealing any more. The observation of a delay of Co oxidation complies well with the picture that, first, oxygen is accumulated in the support by thickening the alumina support, and only then the supported particles are oxidized.

To gather information about the metal particle surface sites and species, IRAS in the range of the vibrational frequencies of CO probe molecules was used. The particles were saturated

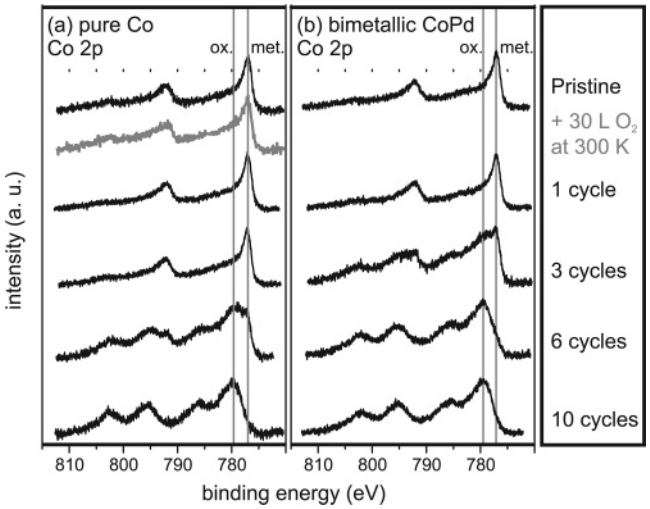

Figure 3. Co 2p XP spectra for (a) 0.2 nm Co and (b) 0.2 nm Co + 0.1 nm Pd deposited on alumina, after exposure to a small dose of oxygen and after cycles of oxygen exposure (30 langmuirs O_2 at 300 K) and annealing (530 K). (a) XPS does not show any indication of particle oxidation after a small oxygen exposure, in contrast to TPD (Figure 2) and FMR (see Figure 5). For pure Co particles a line shift is observable only after six cycles, indicating irreversible oxidation of the particles. After 10 cycles the process seems to be complete. Probably, oxygen is transferred to the supporting NiAl support during annealing only for the first cycles, resulting in continued growth of the alumina film. After the film has reached a certain thickness, diffusion of oxygen is inhibited and the particles are oxidized. (b) For particles covered with an incomplete Pd shell the line shift already occurs after three cycles and seems to be complete after six cycles, indicating that the particle oxidation has required less oxygen. An incomplete shell seems to act as a promoter for the oxygen uptake.

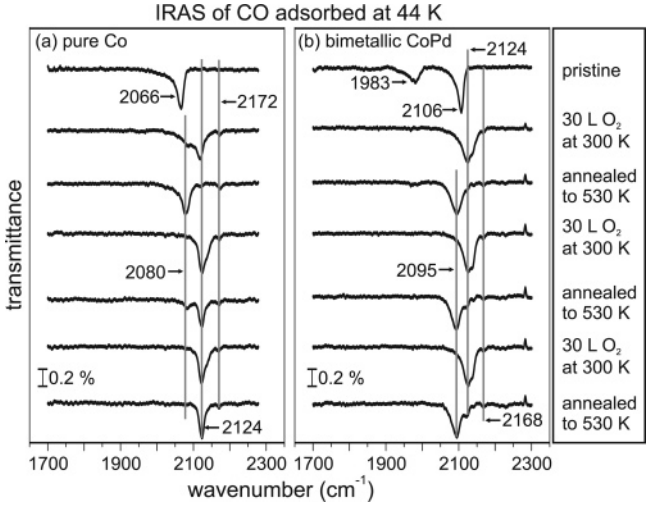

Figure 4. IR spectra for CO on (a) 0.2 nm Co and (b) 0.2 nm Co + 0.1 nm Pd treated with cycles of oxygen exposure and annealing reveal surface species. (a) For pristine particles a peak at 2066 cm^{-1} with a shoulder on the low-energy side is detected. The peak can been attributed to Co carbonyls and the shoulder belongs to terminally bonded CO on Co. Oxygen exposure leads to features at 2080 and 2124 cm^{-1}. The latter vanishes after annealing and is therefore assigned to CO on oxidic Co. The peaks at 2066 and 2080 cm^{-1} belong to the same species; the shift occurs due to remaining oxygen on the surface. After a few cycles only the 2124 cm^{-1} peak is present, indicating a persistent oxygen species. The band at 2172 cm^{-1} visible in all spectra belongs to CO on the alumina support. (b) The spectra for bimetallic particles are dominated by CO on Pd: The bands at 2106 and 2095 cm^{-1} can be attributed to CO on atop-Pd sites. The peak for on top CO shifts to ∼2128 due to coadsorbed oxygen. The shift is completely reversible via oxygen exposure and annealing. As the number of cycles is increased, a peak at 2124 cm^{-1} remains after annealing, indicating the same persistent oxygen species on Co as in the case of pure particles (see a). Small features at 1983 and 1943 cm^{-1} indicate adsorption on the Pd bridge and 3-fold hollow sites which vanish after a few cycles, suggesting a blocking of these sites by remaining oxygen.

with CO at 44 K after each oxygen exposure and each annealing step within a cycle, and IR spectra were recorded at the same temperature. Figure 4a displays the data for pure Co deposits. The spectrum for pristine Co particles in the top panel shows a peak at ∼2066 cm^{-1} with a shoulder on the low-energy side and a band at ∼2172 cm^{-1}. In comparison with previous work, we assign the peak at 2066 cm^{-1} to Co carbonyl species ($Co(CO)_n$) with $n \geq 3$ and the shoulder at lower wavenumbers to terminally bonded CO.[47,53] Terminally bonded CO is found at ∼2012 cm^{-1} on Co(0001),[54] at ∼1972−2020 cm^{-1} on Co($10\bar{1}0$),[55] and ∼1980 cm^{-1} on Co($10\bar{1}2$),[56] while bands between 2060 and 2100 cm^{-1} observed for CO on silica-supported Co catalysts were assigned to carbonyl species.[57] Although the carbonyl band completely dominates the IR spectrum for pristine Co particles in our data due to a high dynamic dipole moment,[47] it is a minority species according to TPD (see Figure 2, spectrum 1 and discussion). When the particles are exposed to O_2 at RT, a peak at 2124 cm^{-1} is observed in the IR spectrum for subsequently adsorbed CO, while some carbonyl-related intensity remains (see Figure 4a). The latter recovers after annealing to 530 K to a full peak at ∼2080 cm^{-1}, while the peak at 2124 cm^{-1} has disappeared. After a few cycles of oxygen exposure and annealing, however, the feature at 2124 cm^{-1} dominates all spectra and the carbonyl signal at 2080 cm^{-1} hardly recovers after annealing. Assigning the peak at 2124 cm^{-1} to CO on oxygen-terminated Co, we find a strong correspondence between IRAS and TPD data. Note, however, that the IR stretching frequency of CO bound to oxidized Co is shifted as compared to stoichiometric CoO films showing a CO stretching frequency of 2145 cm^{-1} for CoO(100) and 2169 cm^{-1} for CoO(111).[58] While XPS indicates a majority of metallic Co species in the particles, both IRAS and TPD reveal that the binding energy of CO at the particle surface is dominated by cobalt oxide species already after at few cycles of oxygen exposure and annealing. It should be noted that the shift of the carbonyl-related band from 2066 to 2080 cm^{-1} after oxygen exposure and annealing indicates changes in the CO−particle interaction. The IR-band observable at 2172 cm^{-1} is attributable to CO adsorption on the alumina film.[59]

So far, we have demonstrated that removing a large part of the oxygen from the particles via heating does not restore the adsorption behavior characteristic for metallic Co, hinting toward the irreducible formation of a surface oxide shell. If the surface oxide shell was CoO, however, XPS should detect the oxidized Co species because ∼40% of the Co atoms are located at surface sites of the particles.

To probe the entire particle volume by an alternative technique, FMR measurements were performed. The result for a Co deposition of 0.4 nm exposed to O_2 at 300 K is shown by the black, solid line in Figure 5, where the relative FMR intensity is plotted vs the total oxygen dose. Metallic particles are ferromagnetic, whereas cobalt oxide does not contribute to the FMR intensity. The FMR signal decreases in intensity for an oxygen dose of ∼20 langmuirs already significantly and vanishes completely for ∼90 langmuirs, suggesting oxidation of the nanoparticles, while XPS shows mostly metallic Co for such amounts of O_2. Obviously, exposing the particles to oxygen has a huge influence not only on surface properties but also on bulk properties, such as the magnetic moment, revealing that a surface CoO shell on top of a metallic core cannot serve as an adequate model for our observations.

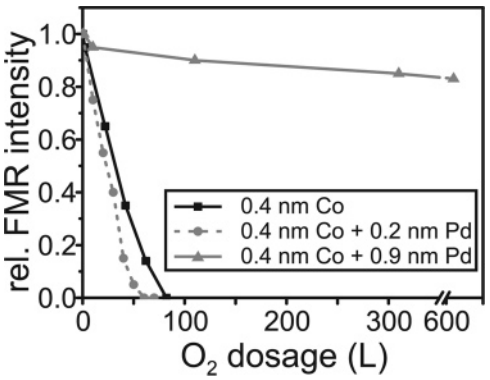

Figure 5. FMR intensity versus oxygen exposure at 300 K for different particles: pure Co, Co with an incomplete Pd shell (0.4 nm Co + 0.2 nm Pd), and Co with a complete Pd shell (0.4 nm Co + 0.9 nm Pd). For pure and incompletely covered Co, exposure to small doses of oxygen results in a complete loss of the FMR signal, revealing that small amounts of oxygen affect not only the adsorption behavior but also certain bulk properties such as the magnetism. The FMR signal of Co particles with an incomplete Pd shell vanishes at smaller amounts of oxygen than that of pure Co particles, indicating Co oxidation promotion by an incomplete Pd shell (only metallic Co contributes to the FMR intensity). In the case of Co particles with a complete Pd shell, oxygen exposure has a fairly reduced influence on the FMR signal, indicating that the complete Pd shell protects Co from being oxidized.

The apparent contradiction of XPS and FMR results rather points at the formation of non-stoichiometric surface and subsurface cobalt oxide, probably in small amounts. Brundle et al. dosed 10 langmuirs of O_2 at 300 K to polycristalline Co *without* detecting a significant XPS peak shift for the Co 2p signal.[34] They observed, however, two peaks in the O1s binding energy region, assigning the first one at ~529.5 eV to cobalt oxide and a second small one at ~531.3 eV to oxygen in the surface region, i.e., surface and subsurface species. A quite similar result has been reported by Klingenberg et al.[31] for a Co($11\bar{2}0$) surface. Exposure to 12 langmuirs of oxygen at 100 K leads to no significant shift of the Co 2p state but to the detection of two oxygen related signals, cobalt oxide at ~529.5 eV and an additional species at ~530.4 eV, associated with disordered (located at defect sites) or non-stoichiometric oxygen. Comparable results are reported for Co films on Fe(001) by Valeri et al.[35] Unfortunately, in our XPS data the O1s binding energy region is dominated by the alumina support so that the amount of oxygen in the Co particles cannot be estimated. Nevertheless, the large width of the CO TPD signal and the red-shifted CO IR frequency as compared to a stoichiometric CoO film[58] clearly point to a non-stoichiometric oxide phase. Thus, in summary the combined TPD, IRAS, FMR, and XPS results suggest that a stable non-stoichiometric subsurface or subsurface *and* surface oxygen species remains in the particles after oxygen exposure and annealing.

As already mentioned in the introduction, the addition of palladium is known to be beneficial for the catalytic behavior of Co in terms of the Fischer−Tropsch process. In the remainder, the interaction of oxygen with bimetallic Co−Pd will be discussed in comparison to the XPS, CO-IRAS, and FMR results for pure Co particles. We deposited 0.1 nm of Pd on top of 0.2 nm Co, leading to Co core particles with an incomplete Pd shell. The latter statement is based on previous TPD and IR results and is consistent with a simple geometric core shell model using particle sizes deduced from STM.[41,42,53] Afterward the sample was treated with the same cycles of oxygen exposure and annealing as described above. XPS data of the Co 2p states are shown in Figure 3b. The spectrum for pristine nanoparticles indicates a metallic Co core, and one cycle does not induce significant changes, as for monometallic particles. In contrast to pure Co deposits, however, there is a discernible oxide component after three cycles, already (see Figure 3a). After six cycles, the Co 2p peaks have shifted completely to the positions for cobalt oxide, whereas at least ten cycles were necessary to achieve the same for monometallic particles. During the treatment, the Pd 3d XPS signal remains essentially unaltered (not shown), indicating that Pd is not oxidized, as expected, and the alumina film thickens as discussed before. Obviously, the incomplete Pd shell enhances the oxidation of the Co core, presumably by continuously supplying atomic oxygen to the Co and the support. Since the Pd shell remains metallic during a cycle, O_2 is efficiently dissociated while in the case of pure Co particles, their cumulative oxidation reduces the catalytic activity of their surface toward O_2 dissociation.

The influence of cycles of oxygen exposure and annealing on CO adsorption on the bimetallic particles has been examined by means of IRAS after saturating the surface with CO at 44 K for each spectrum (Figure 4b). For pristine particles, adsorption bands at 2106, 1983, and 1942 cm^{-1} are observable. By comparison with spectra for monometallic Pd crystallites[38,40] the first band can be attributed to CO terminally bonded to Pd, the second and third to bridge sites. As mentioned before, the small feature at 2168 cm^{-1} represents CO adsorption on the alumina film.[59] An IR peak representing carbonyl species on Co cannot be detected, although the Pd shell is not complete and the carbonyl band dominates the IR spectra for pure Co particles (see Figure 4a). It was shown that the low-coordinated Co sites, acting as formation sites for carbonyls, are also preferential nucleation sites for Pd.[53] After oxygen exposure, only a broad band at 2124 cm^{-1} appears, which vanishes after annealing to 530 K, as in the case of the pure Co particles. The peak at 2095 cm^{-1}, present after annealing, is assigned to terminally bonded CO on Pd, because of the close proximity to the original band at 2106 cm^{-1}. Another oxygen exposure restores the band at 2124 cm^{-1}, but this time with a discernible shoulder at 2128 cm^{-1}. The data suggest that for bimetallic Pd−Co particles the band at 2124 cm^{-1} does not only represent CO on oxygen-treated Co but also CO adsorption on Pd-atop sites with coadsorbed oxygen, in agreement with literature.[60] This band can be reversibly shifted between 2095 and 2124 cm^{-1} by oxygen exposure and annealing cycles up to 530 K, presumably because the CO is oxidized by the coadsorbed oxygen during annealing, clearing the Pd sites of oxygen. This is valid only for the atop-CO species, because CO on Pd bridge sites is not detected after a few cycles. These sites are probably blocked by remaining oxygen even after annealing. It can be seen that part of the 2124 cm^{-1} signal remains visible after several cycles even after annealing. Very likely, this part represents CO on oxygen-treated Co, suggesting that annealing does not restore the metallicity of the particles, in agreement with the results discussed for the monometallic Co particles.

The effect of oxygen exposure on the magnetic moment of the bimetallic particles has been investigated by FMR spectroscopy. Figure 5 shows the relative FMR intensity versus the oxygen dosage for different particle ensembles. As already discussed above, for pure Co (0.4 nm) the signal decreases as the total oxygen dose at 300 K is increased. With 0.2 nm Pd forming an incomplete shell on 0.4 nm Co, the slope of the FMR decrease with respect to the O_2 dose is steeper, and the FMR signal vanishes for ~60 langmuirs as compared to ~90 langmuirs for the pure Co particles, indicating a more efficient

oxygen uptake of the Co core. This is in correspondence with the XPS results. In contrast, the Co core is hardly oxidized when covered with a complete Pd shell, prepared by deposition of 0.9 nm Pd on 0.4 nm Co. The observed loss of FMR intensity even for large oxygen doses of more than 500 langmuirs is less than 20%. Probably due to slow oxygen diffusion in Pd, the complete Pd shell inhibits oxygen uptake by the Co core, while a fragmentary Pd shell promotes oxygen transfer to the Co, presumably because O_2 is continuously dissociated at the metallic Pd shell during the cycles of oxygen exposure and annealing.

Conclusions

The interaction of oxygen with Co and Co−Pd core−shell nanoparticles has been studied under UHV conditions using XPS, IRAS of CO, CO−TPD, and FMR spectroscopy. For large oxygen amounts (1000 langmuirs) all methods agree on the formation of oxidized Co particles, while exposure to smaller amounts (50 langmuirs) leads to the apparent contradiction that XPS suggests basically metallic particles, whereas TPD as well as FMR indicate oxidized ones. This discrepancy between XPS and the latter techniques is due to the formation of small amounts of non-stoichiometric surface and subsurface oxygen in the particles. Such phenomena are currently intensively discussed in the literature to have a significant impact on the catalytic properties of metal catalysts (see, e.g., ref 61). Upon annealing, oxygen is transferred from the particles to the alumina support, which grows in thickness until this reaction is limited by diffusion, and the particles are irreversibly oxidized.

In comparison, Co particles with an incomplete Pd shell are oxidized more readily than the monometallic Co particles. Conversely, under reductive conditions these systems are also more reactive toward CoO reduction. This is interesting for Fischer−Tropsch catalysts where Co oxidation was found to cause deactivation of supported Co particles[16−19] and Pd is added to overcome this problem.[20−22] In case Pd forms a closed shell around Co particles, the oxidation is essentially inhibited, because of the limited oxygen diffusion through Pd at 300 K.

With respect to the Fischer−Tropsch reaction it is interesting to investigate the CO cleavage reaction, which is considered an important pathway for the Fischer−Tropsch process, with respect to the oxidation state of the Co particles. Corresponding results will be published elsewhere.[62] It is important to bear in mind than all the investigations described in this report are done under ultrahigh-vacuum conditions. Catalytic tests on morphologically similar systems under ambient pressure conditions have recently been performed to shed light on the reactivity of such model systems under ambient pressure conditions.[63,64]

Acknowledgment. We thank the Deutsche Forschungsgemeinschaft for funding this work within the priority program (SPP) 1091 and the SFB 290 (TP A9). Further support was provided by the Max-Planck-Gesellschaft. A.F.C. and M.S. thank the Alexander von Humboldt Foundation for a support. O.M. acknowledges support from INTAS (Grant 03-55-981).

References and Notes

(1) Wirl, F. *Eng. Costs Prod. Econ.* **1985**, *9*, 105−111.
(2) Wilhelm, D. J.; Simbeck, D. R.; Karp, A. D.; Dickenson, R. L. *Fuel Process. Technol.* **2001**, *71*, 139−148.
(3) Kruglyakova, R.; Gubanov, Y.; Kruglyakov, V.; Prokoptsev, G. *Continental Shelf Res.* **2002**, *22*, 2395−2407.
(4) Maestro, A.; Barnolas, A.; Somoza, L.; Lowrie, A.; Lawton, T. *Mar. Geol.* **2002**, *186*, 351−368.
(5) St. George, J. D.; Barakat, M. A. *Int. J. Coal Geol.* **2001**, *45*, 105−113.
(6) Wegrzyn, J. E.; Mahajan, D.; Gurevich, M. *Catal. Today* **1999**, *50*, 97−108.
(7) Milkov, A. V. *Mar. Geol.* **2000**, *167*, 29−42.
(8) Taylor, M. H.; Dillon, W. P.; Pecher, I. A. *Mar. Geol.* **2000**, *164*, 79−89.
(9) Hovland, M.; Gallagher, J. W.; Clennell, M. B.; Lekvam, K. *Mar. Petrol. Geol.* **1997**, *14*, 245−255.
(10) Vosloo, A. C. *Fuel Process. Technol.* **2001**, *71*, 149−155.
(11) BP statistical review of world energy, 2001.
(12) BP brochure: Cool future for gas, 2001.
(13) Fischer, F.; Tropsch, H. *Brennst.-Chem.* **1926**, *7*, 97−104.
(14) Schulz, H. *Appl. Catal., A* **1999**, *186*, 3−17.
(15) Davis, B. H. *Fuel Process. Technol.* **2001**, *71*, 157−166.
(16) Jacobs, G.; Patterson, P. M.; Yongqing, Z.; Tapan, D.; Jinlin, L.; Davis, B. H. *Appl. Catal., A* **2002**, *233*, 215−226.
(17) Hilmen, A. M.; Schanke, D.; Hanssen, D.; Holmen, A. *Appl. Catal., A* **1999**, *186*, 169−188.
(18) Crajé, M. W. J.; van der Kraan, A. M.; van de Loosdrecht, J.; van Berge, P. J. *Catal. Today* **2002**, *71*, 369−379.
(19) van Berge, P. J.; van de Loosdrecht, J.; Barradas, S.; van der Kraan, A. M. *Catal. Today* **2000**, *58*, 321−334.
(20) Guczi, L.; Borkó, L.; Schay, Z.; Bazin, D.; Mizukami, F. *Catal. Today* **2001**, *65*, 51−57.
(21) Tsubaki, N.; Sun, S.; Fujimoto, K. *J. Catal.* **2001**, *199*, 236−246.
(22) Guczi, L.; Schay, Z.; Stefler, G.; Mizukami, F. *J. Mol. Catal. A: Chem.* **1999**, *141*, 177−185.
(23) Idriss, H.; Diagne, C.; Hindermann, J. P.; Kinnemann, A.; Barteau, M. A. *Proceedings, 10th International Congress on Catalysis*, Budapest, 1992; Elsevier: Amsterdam, New York; 1193, p 2119.
(24) Kapoor, M. P.; Lapidus, A. L.; Krylova, A. Y. *Proceedings, 10th International Congress on Catalysis*, Budapest, 1992; Elsevier: Amsterdam, New York; 1993, p 2741.
(25) Juszczyk, W.; Karpinski, Z.; Lomot, D.; Pielaszek, J.; Paal, Z.; Stakheev, A. Y. *J. Catal.* **1993**, *142*, 617−629.
(26) Noronha, F. B.; Schmal, M.; Nicot, C.; Moraweck, B.; Frety, R. *J. Catal.* **1997**, *168*, 42−50.
(27) Bischoff, S.; Weigt, A.; Fujimototo, K.; Lücke, B. *J. Mol. Catal. A: Chem.* **1995**, *95*, 259.
(28) Guczi, L.; Borkó, L. *Catal. Today* **2001**, *64*, 91−96.
(29) Bridge, M. E.; Lambert, R. M. *Surf. Sci.* **1979**, *82*, 413−424.
(30) Castro, G. R.; Küppers, J. *Surf. Sci.* **1982**, *123*, 456−470.
(31) Klingenberg, B.; Grellner, F.; Borgmann, D.; Wedler, G. *Surf. Sci.* **1993**, *296*, 374−382.
(32) Klingenberg, B.; Grellner, F.; Borgmann, D.; Wedler, G. *Surf. Sci.* **1997**, *383*, 13−24.
(33) Gierer, M.; Over, H.; Rech, P.; Schwarz, E.; Christmann, K. *Surf. Sci. Lett.* **1997**, *370*, L201−L206.
(34) Brundle, C. R.; Chuang, T. J.; Rice, D. W. *Surf. Sci.* **1976**, *60*, 286−300.
(35) Valeri, S.; Borghi, A.; Gazzadi, G. C.; di Bona, A. *Surf. Sci.* **1999**, *423*, 346−356.
(36) Jaeger, R. M.; Kuhlenbeck, H.; Freund, H.-J.; Wuttig, M.; Hoffmann, W.; Franchy, R.; Ibach, H. *Surf. Sci.* **1991**, *259*, 235−252.
(37) Hill, T.; Mozaffari-Afshar, M.; Schmidt, J.; Risse, T.; Stempel, S.; Heemeier, M.; Freund, H.-J. *Chem. Phys. Lett.* **1998**, *292*, 524−530.
(38) Bäumer, M.; Frank, M.; Heemeier, M.; Kühnemuth, R.; Stempel, S.; Freund, H.-J. *Surf. Sci.* **2000**, 456−454; 957−962.
(39) Bäumer, M.; Freund, H.-J. *Prog. Surf. Sci.* **1999**, *61*, 127−198.
(40) Frank, M.; Bäumer, M. *Phys. Chem. Chem. Phys.* **2000**, *2*, 3723−3737.
(41) Heemeier, M.; Carlsson, A. F.; Naschitzki, M.; Schmal, M.; Bäumer, M.; Freund, H.-J. *Angew. Chem., Int. Ed.* **2002**, *41*, 4073−4076.
(42) Carlsson, A. F.; Naschitzki, M.; Bäumer, M.; Freund, H.-J. *J. Phys. Chem. B* **2003**, *107*, 778−785.
(43) Heemeier, M.; Stempel, S.; Shaikhutdinov, S. K.; Libuda, J.; Bäumer, M.; Oldman, R. J.; Jackson, S. D.; Freund, H.-J. *Surf. Sci.* **2003**, *523*, 103−110.
(44) Hill, T.; Risse, T.; Freund, H.-J. *J. Chem. Phys.* **2005**, *122*, 164704.
(45) Hill, T.; Mozaffari-Afshar, M.; Schmidt, J.; Risse, T.; Freund, H.-J. *Surf. Sci.* **1999**, *429*, 246−254.
(46) Schmidt, J.; Risse, T.; Hamann, H.; Freund, H.-J. *J. Chem. Phys.* **2002**, *116*, 10861−10868.
(47) Risse, T.; Carlsson, A. F.; Bäumer, M.; Klüner, T.; Freund, H.-J. *Surf. Sci. Lett.* **2003**, *546*, L829−L835.
(48) Lahtinen, J.; Vaari, J.; Kauraala, K. *Surf. Sci.* **1998**, *418*, 502−510.
(49) Carlsson, A. F.; Naschitzki, M.; Bäumer, M.; Freund, H.-J. *Surf. Sci.* **2003**, *545*, 143−153.
(50) Freund, H.-J. *Faraday Discuss.* **1999**, *114*, 1−31.
(51) Shaikhutdinov, S.; Heemeier, M.; Hoffmann, J.; Meusel, I.; Richter, B.; Bäumer, M.; Kuhlenbeck, H.; Libuda, J.; Freund, H.-J.; Oldman, R.; Jackson, S. D.; Konvicka, C.; Schmid, M.; Varga, P. *Surf. Sci.* **2002**, *501*, 270−281.

(52) Winkler, A.; Borchert, A.; Al-Shamery, K. *Surf. Sci.* **2006**, *600*, 3036−3044.

(53) Carlsson, A. F.; Bäumer, M.; Risse, T.; Freund, H.-J. *J. Chem. Phys.* **2003**, *119*, 10885.

(54) Beitel, G. A.; Laskov, A.; Oosterbeek, H.; Kuipers, E. W. *J. Phys. Chem.* **1996**, *100*, 12494−12502.

(55) Toomes, R. L.; King, D. A. *Surf. Sci.* **1996**, *349*, 1−18.

(56) Geerlings, J. J. C.; Zonnevylle, M. C.; de Groot, C. P. M. *Surf. Sci.* **1991**, *241*, 315−324.

(57) Heal, M. J.; Leisegang, E. C.; Torrington, R. G. *J. Catal.* **1978**, *51*, 314−325.

(58) Haβel, M. Ph.D. thesis, Ruhr-Universität Bochum, 1994.

(59) Zecchina, A.; Scarano, D.; Bordiga, S.; Ricchiardi, G.; Spoto, G.; Geobaldo, F. *Catal Today* **1996**, *27*, 403−435.

(60) Stuve, E. M.; Madix, R. J.; Brundle, C. R. *Surf. Sci.* **1984**, *146*, 155−178.

(61) Penner, S.; Wang, D.; Jenewein, B.; Gabasch, H.; Klötzer, B.; Knop-Gericke, A.; Schlögl, R.; Hayek, K. *J. Chem. Phys.* **2006**, *125*, 094703.

(62) Nowitzki, T.; Zielasek, V.; Risse, T.; Bäumer, M. Manuscript in preparation.

(63) Borchert, H.; Jürgens, B.; Zielasek, V.; Rupprechter, G.; Giorgio, S.; Henry, C. R.; Bäumer, M. *Catal, J.* **2007**, *247*, 145−154.

(64) Borchert, H.; Jürgens, B.; Zielasek, V.; Giorgio, S.; Henry, C. R.; Bäumer, M. Manuscript in preparation.